7044 J. Med. Chem. 2009, 52, 7044–7053
DOI: 10.1021/jm900681h

Journal of Medicinal Chemistry Article

Discovery and Optimization of Chromenotriazolopyrimidines as Potent Inhibitors of the Mouse Double Minute 2−Tumor Protein 53 Protein−Protein Interaction

John G. Allen,*,† Matthew P. Bourbeau,† G. Erich Wohlhieter,† Michael D. Bartberger,† Klaus Michelsen,† Randall Hungate,† Robert C. Gadwood,‡ Rick D. Gaston,‡ Bruce Evans,‡ Larry W. Mann,‡,¶ Michael E. Matison,‡ Stephen Schneider,§ Xin Huang,§ Dongyin Yu,∥ Paul S. Andrews,§ Andreas Reichelt,† Alexander M. Long,§ Peter Yakowec,§ Evelyn Y. Yang,⊥ Tani Ann Lee,∥,▽ and Jonathan D. Oliner∥

†*Chemistry Research and Discovery, Amgen Inc., One Amgen Center Drive, Thousand Oaks, California 91320,* ‡*Kalexsyn Inc. 4502 Campus Drive, Kalamazoo, Michigan 49008,* §*Chemistry Research and Discovery, Amgen, Inc., One Kendall Square, Cambridge Massachusetts 02139,* ⊥*Protein Science, Amgen Inc., One Amgen Center Drive, Thousand Oaks, California 91320, and* ∥*Oncology Research, Amgen Inc., One Amgen Center Drive, Thousand Oaks, California 91320.* ¶ *Current address: Pfizer Animal Health, 333 Portage Street, Kalamazoo, Michigan, 49007.* ▽ *Current address: Prometheus Laboratories, Inc., San Diego, CA, 92121.*

Received May 21, 2009

Tumor protein 53 (p53) is a critical regulator of cell cycle and apoptosis that is frequently disabled in human tumors. In many tumor types, p53 is deleted or mutated, but in others p53 is inactivated by overexpression or amplification of its negative regulator mouse double minute 2 (MDM2). A high-throughput screening effort identified 6,7-bis(4-bromophenyl)-7,12-dihydro-6*H*-chromeno[4,3-*d*]-[1,2,4]triazolo[1,5-*a*]pyrimidine as a potent inhibitor of the MDM2−p53 protein−protein interaction. This screening hit was found to be chemically unstable and difficult to handle due to poor DMSO solubility. Co-crystallization with the target protein helped to direct further optimization and provided a tractable lead series of novel MDM2−p53 inhibitors. In cellular assays, these compounds were shown to upregulate p53 protein levels and p53 signaling and to cause p53-dependent inhibition of proliferation and apoptosis.

Introduction

An important cell cycle regulator, p53[a], promotes the transcription of genes that control cell cycle arrest and apoptosis.[1] p53 knockout mice show a high incidence of spontaneous tumors,[2] and cancer patients with inactivated p53 have been reported to exhibit a poor prognosis.[3] In approximately half of all human tumors, p53 is inactivated by mutation or deletion.[4] In tumors that harbor wild-type p53, p53 is often downregulated by other mechanisms, for example, by overexpression[5] or amplification[6] of MDM2.[7] MDM2 inhibits p53 by binding to and blocking the p53 transactivation domain.[8] MDM2 is also involved in the nuclear export of p53. In addition, MDM2 has enzymatic activity as an E3 ligase and can ubiquitinate p53,[9] thereby targeting p53 for proteosomal degradation. Under non-stressed conditions, MDM2 in turn is tightly regulated by p53 via promotion of MDM2 transcription in an autoinhibitory feedback loop.[10] Activation of the p53 pathway in p53 wild-type cancer by inhibition of MDM2 has been proposed as a novel anticancer therapeutic strategy.[11] Further, in patients with p53-inactivated tumors, stabilization of wild-type p53 in normal tissues by MDM2 inhibition might allow selective protection of normal tissues from mitotic poisons.[12]

Although protein−protein interactions have been considered challenging targets for drug discovery,[13] the MDM2−p53 complex has been characterized by an MDM2 hot spot[14] occupied by critical p53 residues Phe19, Trp23, and Leu26. Furthermore, a number of small molecules[15] including *cis*-imidazolines, benzodiazepinediones, spiro-oxindoles, and peptides[16] that bind human MDM2 at the p53 binding site and disrupt the MDM2−p53 binding interaction have been described and recently reviewed.[17] In an HTRF-based high-throughput screen of ca. 1.4 million internal library compounds, FRET was quenched in a concentration-dependent manner by chromenotriazolopyrimidine **1** (IC_{50} = 3.88 ± 1.48 μM).[18] Surface plasmon resonance (SPR) direct binding experiments demonstrated that **1** reversibly bound MDM2 ($K_d \approx 11$ μM) but not p53, GST, or the chip matrix, indicating that the FRET quenching behavior of **1** was specific to MDM2 binding. Subsequent characterization found that **1** was a racemic mixture of *syn* and *anti* diastereomers (1:1:3:3 **1a**/**1b**/**1c**/**1d**) as shown in Table 1. Chiral SFC chromatographic separation, followed by determination of the absolute configuration of all four stereoisomers by vibrational circular dichroism (VCD) and retesting, demonstrated that only the *syn*-(6*R*,7*S*) stereoisomer **1a** was responsible for activity

*To whom correspondence should be addressed. Phone: (805) 313-5257. Fax: (805) 480-1337. E-mail: johallen@amgen.com.

[a] Abbreviations: DMSO, dimethyl sulfoxide; FRET, Förster resonance energy transfer; GST, glutathione S-transferase; MDM2, human mouse double minute 2; HTRF, homogeneous time-resolved fluorescence; p53, tumor protein 53; SFC, supercritical fluid chromatography; VCD, vibrational circular dichroism; SPR, surface plasmon resnonance; LE, ligand efficiency; ATP, adenosine triphosphate; UBE1, ubiquitin-activating enzyme 1; UbcH5b, ubiquitin-conjugating enzyme homologue 5b; SD, standard deviation; TA, transcription activation; BrdU, 5-bromo-2-deoxyuridine; GAPDH, glyceraldehyde 3-phosphate dehydrogenase; RFU, relative fluorescence units; BSA, bovine serum albumin; RT-PCR, reverse transcription polymerase chain reaction; FACS, fluorescence-activated cell sorting; IC_{50}, half-maximal inhibitory concentration; K_d, dissociation constant.

 Published on Web 10/26/2009

disrupting the MDM2−p53 interaction (IC_{50} = 1.23 ± 0.82 μM). Concurrently, **1a** did not inhibit the ubiquitin ligase activity of MDM2 (IC_{50} > 50 μM). Although the molecular weight of **1a** was high for a lead compound (MW = 536.22 Da), it has been reported that inhibitors of protein−protein interactions may require larger molecules to be effective.[13b] In this regard, the ligand efficiency[19] of **1a** (LE = 0.26 kcal/mol per non-hydrogen atom) was comparable to that of other known small molecule inhibitors of protein−protein interactions.[20] During this work, isomers of **1** were observed to be poorly soluble in organic solvents including DMSO.

Table 1. High-Throughput Screening Hit **1** and Its Stereoisomeric Components. [a]

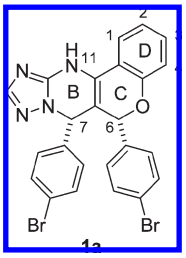

compound	stereochemistry	HTRF IC_{50} (μM)
1	mixture[b]	3.88 ± 1.48
1a	(6*R*,7*S*)	1.23 ± 0.82
1b	(6*S*,7*R*)	> 100
1c	(6*S*,7*S*)	> 100
1d	(6*R*,7*R*)	> 100

[a] Compound numbering as used throughout the discussion is indicated. [b] Compound **1** was discovered as a 1:1:3:3 mixture of **1a**/**1b**/**1c**/**1d**.

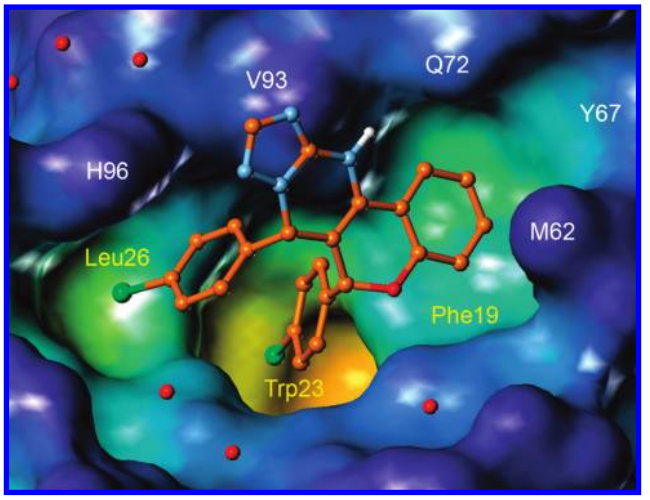

Figure 1. X-ray cocrystal structure of **1a** with human MDM2, colored by cavity depth (PDB code 3JZK). Yellow labels indicate the positions normally occupied by key p53 residues. MDM2 residues are labeled in white. Cocrystallized water molecules are shown in red.

The predicted absolute stereochemistry of **1a** was confirmed by cocrystallization with MDM2 as shown in Figure 1. In comparison with previous MDM2−p53 structural data,[16a] it was seen that **1a** and p53 both bound MDM2 utilizing the same key binding interactions. The C7 aryl group of **1a** was found to occupy the same pocket as Leu26 of p53, while forming a weak π-stacking interaction (ca. 4.0−4.9 Å) with the nearby H96 side chain of MDM2. The C6 aryl group of **1a** overlapped with the Trp23 region of p53, while the D ring of the chromene group interacted with the binding pocket utilized by p53 Phe19. It was hoped that by optimizing interactions within these binding pockets, ligand binding affinity could be improved, leading to more efficient displacement of p53 from MDM2.

Efforts to optimize MDM2 inhibition by chromenotriazolopyrimidines were hindered by chemical instability within the series. It was found that the individual diastereomers of **1** and analogs (data not shown) equilibrated over a period of hours at room temperature in DMSO, resulting in mixtures favoring the thermodynamically more stable *anti* stereoisomers (i.e., **1c** or **1d**). No deuterium incorporation was observed upon equilibration in MeOH-d_4, and racemization was found to occur only at the C6 position (**1a** ↔ **1c** and **1b** ↔ **1d**). Furthermore, pure **1a** and pure **1c** were both found to equilibrate to the same 1:3 *syn*/*anti* ratio. These observations were consistent with the mechanism shown in Scheme 1 wherein opening of the C ring with loss of the phenol leaving group proceeded via enimine **2** as an intermediate. It was envisioned that substitution at N11 might prevent racemization of the C6 carbon as formation of the requisite iminium ion corresponding to **2** would be disfavored. For example, the N-methylated compounds were found to be stable under normal handling and assaying conditions. They were also observed to be much more soluble in organic solvent compared with their des-methyl analogs. Importantly, the N11 methyl group did not diminish MDM2 potency (cf. **1a**, IC_{50} = 1.23 ± 0.02 μM, and **11**, IC_{50} = 1.17 ± 0.30 μM).

A flexible synthesis of the N11 methylated chromenotriazolopyrimidines is shown in Scheme 2.[21] Aldol condensation of a variety of aldehydes **3** and hydroxyacetophenones **4** resulted in hydroxychalcones **5**, which in turn were condensed with neat 4*H*-1,2,4-triazol-3-amine at 160 °C to provide **6** as a mixture of two tautomers. The enamine tautomer **6** could be enriched over the imine tautomer by trituration from chloroform. Condensation with a variety of aldehydes under thermal or acidic conditions via trapping by the phenol gave stereoisomeric mixtures of **7**. In some cases, compounds with the general structure **7** were commercially available. *N*-Methylation provided the 11-methylchromenotriazolopyrimidines as racemic mixtures of thermodynamic *anti* (**8**) and *syn* (**9**−**11**,

Scheme 1

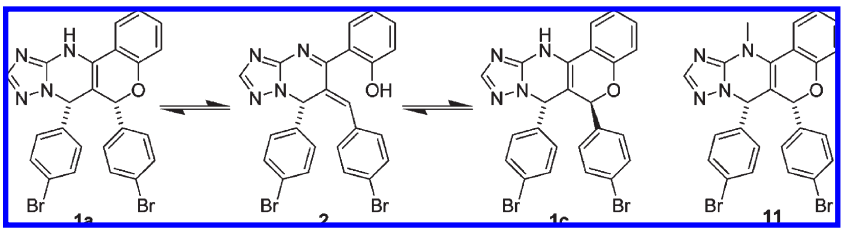

Scheme 2[a]

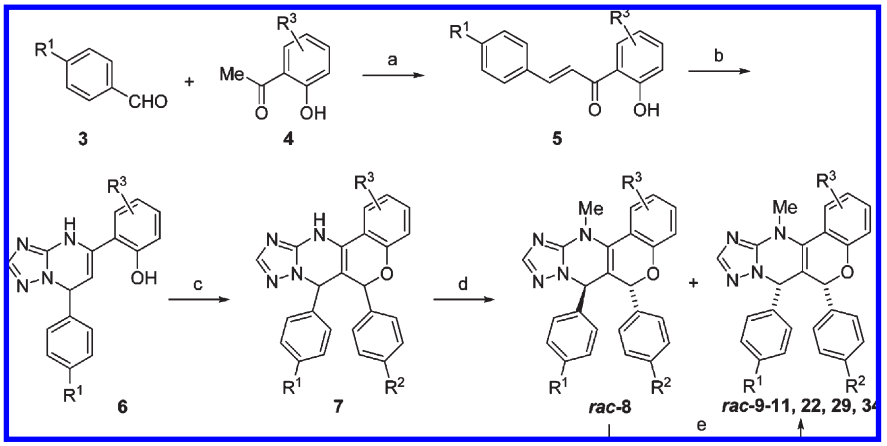

[a] Reagents and conditions: (a) EtOH, KOH, 16 h, rt, 69−93%; (b) 4*H*-1,2,4-triazol-3-amine, 30 min, 160 °C, 53−100%; (c) ArCHO, 10 min, 160 °C, or ArCHO, $Sm(OTf)_3$, TFA, DMF, 3 h, 70 °C, 14−100%; (d) Cs_2CO_3, MeI, 0 °C to rt, 4 h, 1:3 to 10:1 *anti*/*syn* mixture; purification by trituration and/or chromatography 2−77%; (e) 120−160 °C, DMSO, 1−4 h; purification by trituration and/or chromatography.

Scheme 3[a]

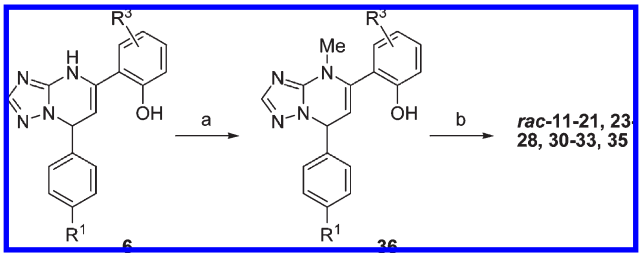

[a] Reagents and conditions: (a) (i) CH_2Cl_2, Et_3N, TBSCl, 16 h, rt, 33−81%; (ii) THF, NaH, CH_3I, 3 h, 0 °C to rt, 27−100%; (iii) 10:1 DMF/water, Cs_2CO_3, rt, 1 h, 43−90%; (b) ArCHO, 10 min, 160 °C, or ArCHO, $Y(OTf)_3$, TFA, 3 h, 80 °C; purification by trituration and/or chromatography 3−50%.

22, **29**, **34**) diastereomers. The final chemical steps were capricious due to variability in the ratio of *syn* (desired) to *anti* diastereomers, and yields were found to be compound-dependent in both the condensation of **6** and methylation of **7**. The *anti* and *syn* diastereomers were separable by trituration or chromatography. Although the *N*-methylated compounds were configurationally stable under normal handling at room temperature, in the cases of an unfavorable *syn*/*anti* ratio, the less active *anti* diastereomers **8** could be reequilibrated at higher temperatures to a *syn*/*anti* mixture and additional *syn* diastereomers could be reisolated.

In addition to variable *syn*/*anti* ratios, incomplete methylation of intermediate **7** was also observed. An alternative to late stage methylation of intermediate **7** involved the similar methylation of **6** following temporary protection of the phenol as the corresponding TBS ether (Scheme 3). Intermediate **36** was then condensed with benzaldehydes under conditions similar to those shown in Scheme 2 to provide (±)-11-methylchromenotriazolopyrimidines (**11**−**21**, **23**−**28**, **30**−**33**, **35**). The *syn*/*anti* ratio did not appear to be strongly affected by choice of either **6** or **36** in the aldehyde condensation reaction. In a head-to-head comparison of **11** prepared either from **7** (method A) or via **36** (method B), overall yields were similar (19% based on **7** vs 29% based on **6**). By variation of benzaldehydes and acetophenones **4**, C-7 and C-6 aryl analogs and D-ring analogs were prepared. In this way, it was possible to explore chromenotriazolopyrimidine interactions

Table 2. C6 and C7 Aryl Ring SAR for Compounds **9**−**21**

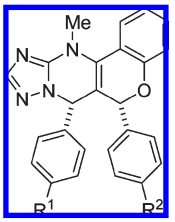

compound[a]	R^1	R^2	HTRF IC_{50} (μM)[b]
9	F	F	14.80 ± 2.0
10	Cl	Cl	1.21 ± 0.10
11	Br	Br	1.17 ± 0.30
12	Br	F	6.57 ± 0.43
13	Br	Cl	0.89 ± 0.20
14	Br	CH_3	4.63 ± 0.92
15	Br	CN	2.08 ± 1.1
16	Br	CCH	2.47 ± 0.68
17	Br	$CCCH_3$	9.07 ± 2.74
18	Br	Et	> 100
19	F	Br	1.88 ± 0.19
20	CH_3	Br	4.74 ± 2.0
21	CN	Br	5.84 ± 5.1

[a] All compounds were racemic. [b] Values reported as mean of at least four experiments, followed by the standard deviation (SD).

in the three major MDM2 binding pockets normally occupied by Leu26, Trp23, and Phe19 of p53.

In an effort to improve physical properties, it was first tested whether aryl substituents lower in weight than bromine might be tolerated (Table 2). Although difluoro analog **9** was found to be less active, dichloro species **10** was equipotent to the parent dibromo compound **11**, while 89 Da lower in molecular weight. Based on the cocrystal structure of **1a** with MDM2, there was interest in probing the deeper Trp23 pocket with R^2 substituents. Again, fluoro analog **12** was less potent, whereas chloro substitution was better tolerated (**13**, 0.89 ± 0.20 μM). The incrementally larger methyl group in **14** caused a sharp decline in potency. It was hoped that linear groups bearing π-character might probe deeper into the pocket and possibly interact with aromatic residues F86 and F91 in this region of the MDM2 protein. Nitrile analog **15** was promising with similar activity (2.08 ± 1.1 μM vs 1.17 ± 0.30 μM for **11**);

however, alkynes **16** and **17** were 2−8-fold less active. Modeling suggested that a small, but potentially accessible, space was located near the bottom of the Trp23 binding pocket. However, compound **18**, bearing an ethyl substituent, disappointingly lacked measurable activity. Next the Leu26 pocket was probed with substituents in the R^1 position. Although activity of the fluoro analog **19** was somewhat diminished (1.88 ± 0.19 μM for **19** vs 1.17 ± 0.30 μM for **11**), fluorine was found to be better tolerated in the Leu26 pocket than in the deeper Trp23 pocket (**19** vs **12**). Methyl and cyano analogs **20** and **21** were 4−5-fold less potent than **11**, a drop in activity similar to that observed for methyl and cyano substitution in the Trp23 pocket (cf. **14** and **15**).

By using differently substituted hydroxyacetophenones (**4**), we were able to probe the Phe19 pocket with substituents on the D-ring (Table 3). The C1 fluoro substituent of **22** may have caused a slight decrease in potency (1.72 ± 0.40 μM for **22** vs 1.17 ± 0.30 μM for **11**), but methoxy (**23**) improved potency by 3.9-fold. The C1 ethoxy appeared to be a neutral substituent with potency of **24** (0.91 ± 0.24 μM) not significantly different from that of **11**. From the cocrystal structure of **1a** with MDM2 and computational modeling, it could be speculated that the improved activity of **23** in particular was less dependent on improved contacts around the methoxy group but rather may have been a result of torsion of the chromenotriazolopyrimidine core due to a 1-OMe/11-Me *meso* interaction to allow improved contacts in the Leu26 and Trp23 pockets. In compounds **25** and **26**, the 2-F and 2-Cl substituents trended toward decreased activity, but 2-Me in **27** provided a 2-fold increase in potency. The cocrystal structure of **1a** with MDM2 showed an extended binding pocket that was available to the C-2 substituent; correspondingly, 2-Et also appeared to be tolerated (**28** was tested with only 25% of the active *syn* diastereomer). The nitrile substituent of **29** was less potent than was expected (3.06 ± 0.15 μM). In contrast the C-3 position was predicted to be the most sterically restricted. Indeed 3-F (**30**) was tolerated, but potency quickly fell off with a 3-Cl substituent (**31**, 13-fold). Compound **32** bearing 4-Cl was also less potent (3.50 ± 0.58 μM for **31** vs 1.17 ± 0.30 for **11**). Compound **33** combined the 1-OMe group of **23** and 2-Me group of **27**, both of which lead to improvements in activity (4- and 2.7-fold, respectively). Unfortunately, this SAR was not additive and resulted in decreased potency (**33**, 3.94 ± 1.12 μM). Similarly, **35** with a 4-Cl substituent in combination with 2-Cl was less potent than either the 2-Cl or 4-Cl alone (> 100 μM for **35** tested as a 1:3 syn/*anti* mixture vs 1.40 ± 0.25 μM for **26** and 3.50 ± 0.58 μM for **32**). Other combinations were more complementary; for example, **34** (0.48 ± 0.02 μM) with 2-methyl-3-fluoro had similar potency to **27** (2-Me, 0.44 ± 0.08 μM) and **30** (3-F, 0.99 (0.15 μM).

Although the compounds compared in Tables 1 and 2 were studied as their racemates, several examples (**10**, **11**, **19**, **23**, **27**) were separated into their individual enantiomers for testing, and the corresponding *anti* enantiomers were also tested. Consistent with **1b**, **1c**, and **1d**, neither the (6*S*,7*R*) nor the *anti* isomers were active under the assay conditions. In the case of **23**, the (6*R*,7*S*) isomer had IC_{50} = 0.20 uM ± 0.011 μM. Resolution of **27** provided the (6*R*,7*S*) isomer (**37**) that had IC_{50} = 0.39 uM ± 0.02 μM. By comparison (4*S*,5*R*)-nutlin-3[15a] had IC_{50} = 0.12 ± 0.05 μM in the HTRF assay.

Cellular upregulation of p53 activity was measured in HCT116 p53 wild-type colorectal cancer cells using a p53-dependent reporter assay. As shown in Figure 2, reporter activity in cells treated with chromenotriazolopyrimidines or with (4*S*,5*R*)-nutlin-3 increased in a concentration-dependent

Table 3. D-Ring SAR for Compounds **22**−**35** Bearing Non-H Substituents at Positions 1−4

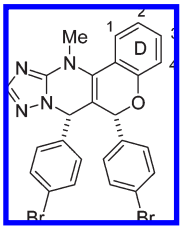

	substituent position				
compound[a]	1	2	3	4	HTRF IC_{50} (μM)[b]
11					1.17 ± 0.30
22	F				1.72 ± 0.40
23	OMe				0.30 ± 0.06
24	OEt				0.91 ± 0.24
25		F			1.73 ± 0.37
26		Cl			1.40 ± 0.25
27		Me			0.44 ± 0.08
28[c]		Et			3.20 ± 1.90
29		CN			3.06 ± 0.15
30			F		0.99 ± 0.15
31			Cl		15.1 ± 7.3
32				Cl	3.50 ± 0.58
33	OMe	Me			3.94 ± 1.12
34		Me	F		0.48 ± 0.02
35[c]		Cl		Cl	> 100

[a] All compounds were racemic. [b] Values reported as the mean of at least four experiments, followed by the standard deviation (SD). [c] Compound was tested as a 1:3 *syn*/*anti* mixture.

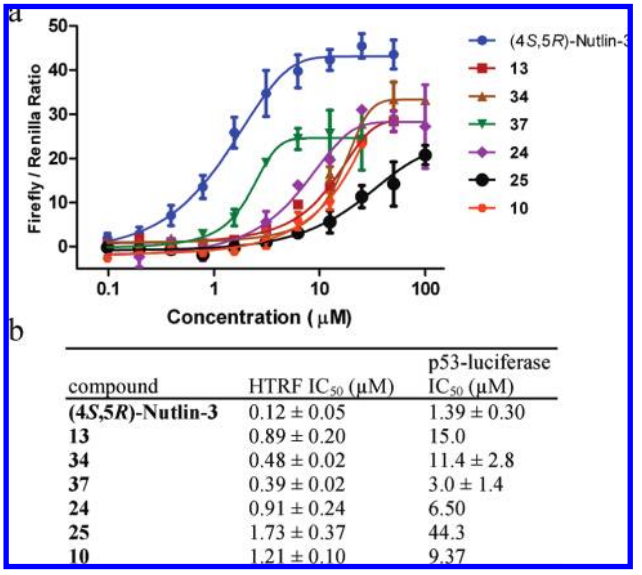

compound	HTRF IC_{50} (μM)	p53-luciferase IC_{50} (μM)
(4*S*,5*R*)-Nutlin-3	0.12 ± 0.05	1.39 ± 0.30
13	0.89 ± 0.20	15.0
34	0.48 ± 0.02	11.4 ± 2.8
37	0.39 ± 0.02	3.0 ± 1.4
24	0.91 ± 0.24	6.50
25	1.73 ± 0.37	44.3
10	1.21 ± 0.10	9.37

Figure 2. MDM2 inhibitors in the chromenotriazolopyrimidine series or (4*S*,5*R*)-nutlin-3 activate a p53-dependent reporter: (a) p53 activation was reported as the ratio of firefly luciferase (under the p53 response element) to *Renilla* luciferase (constitutive expression) in doubly transfected HCT116 cells. Luciferase activities were measured 8 h post-compound treatment. (b) Quantitative biochemical and cellular data. Biochemical values are reported as the mean of at least four experiments followed by SD. For cellular values, SD is provided for measurements with at least n = 2 separate experiments. Each experiment consisted of duplicate wells.

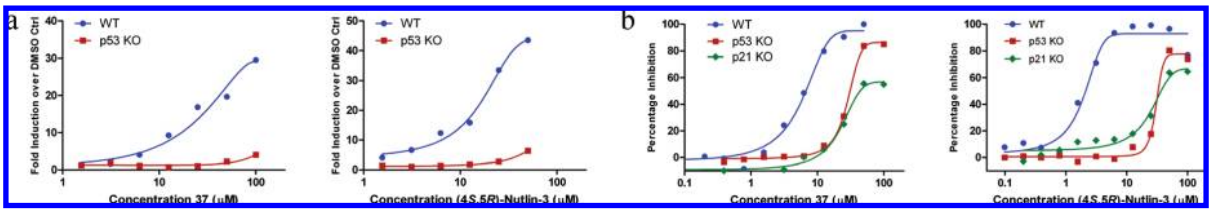

Figure 3. MDM2 inhibitors **37** and (4*S*,5*R*)-nutlin-3 activate p21 and induce p53-dependent inhibition of cell proliferation in HCT116 cells: (a) In HCT116 wild-type and p53-knockout cells that were otherwise isogenic, total RNA was extracted from pools of quadruplicate wells 8 h post-compound treatment and p21 mRNA was measured by real-time RT-PCR. (b) In HCT116 wild-type, p53-knockout, and p21-knockout cells, the percentage of BrdU positive cells was measured from pools of triplicate wells 16 h post-compound treatment by FACS. DMSO controls were designated as 0% inhibition.

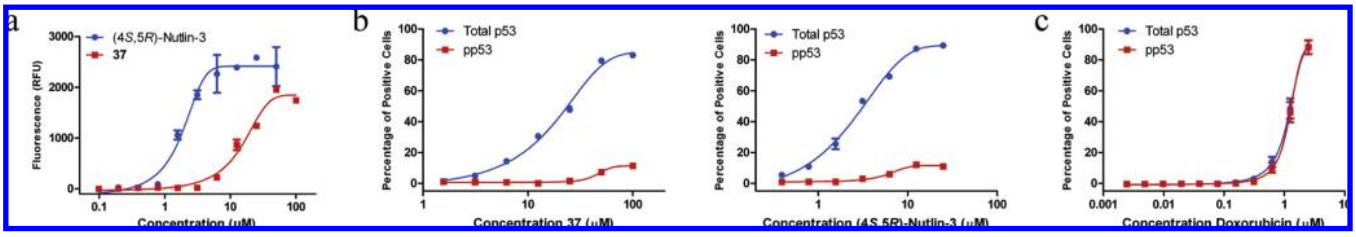

Figure 4. MDM2 inhibitors induce apoptosis and p53 upregulation but not p53 phosphorylation: (a) Compound **37** and (4*S*,5*R*)-nutlin-3 induced apoptosis in SJSA-1 cells. Caspase-3/7 activities were measured 48 h post-compound treatment, and background was subtracted as the average of DMSO controls. (b) MDM2 inhibitors **37** and (4*S*,5*R*)-nutlin-3 induced p53 but not phospho-p53 (Ser15) in HCT116 cells. (c) The cytotoxic agent doxorubicin induced p53 phosphorylation ($IC_{50} \approx 1$ uM). Total p53 and phospho-p53 positive cells were measured 24 h post-compound treatment. Error bars represent SD from duplicate wells.

manner. Biochemical to cellular IC_{50} shifts were 7−26-fold, indicating reasonable cell permeability, but cellular maximum responses were variable. Interestingly, **10**, designed to have improved physical chemical properties, showed one of the smaller cell shifts (7.7-fold). The single active enantiomer **37** resolved from the racemate **27** showed the most potent IC_{50} in the luciferase assay ($IC_{50} = 3.0 \pm 1.4$ μM), and as a chirally pure compound, it was selected for additional mechanism of action studies.

The cyclin-dependent kinase inhibitor p21 is a native transcription target of p53. Exposure of HCT116 cells to **37** or to (4*S*,5*R*)-nutlin-3 resulted in a dose-dependent increase in p21 mRNA (Figure 3a). This effect was dependent on activation of p53 because p21 mRNA did not increase in HCT116 p53 knockout cells.[22a] Both compound **37** and (4*S*,5*R*)-nutlin-3 were also able to inhibit the proliferation of HCT116 cells as measured by BrdU incorporation (Figure 3b). The effect of MDM2 inhibitors on proliferation was dependent on both p53 and p21 because HCT116 knockout cells[22] were less potently inhibited, consistent with p53-induced cell cycle arrest.

Because HCT116 cells are resistant to apoptosis, the apoptosis-sensitive cell line, SJSA-1 (derived from an osteosarcoma), was used for this end point. Apoptosis induction, as measured by caspase-3/7 activation, was concentration-dependent (Figure 4a). In order to rule out nonspecific cytotoxicity as a cause of apoptosis, we measured p53 Ser15 phosphorylation in HCT116 cells. As shown for doxorubicin (Figure 4c), genotoxic drugs promote p53 Ser15 phosphorylation at low concentrations ($IC_{50} \approx 1$ μM), indicating a cytotoxic cell response. In contrast, MDM2 inhibitors **37** and (4*S*,5*R*)-nutlin-3 caused an upregulation in p53 but not the phosphorylation of p53 (Figure 4b). Taken together, the data in Figures 3 and 4 indicate that the chromenotriazolopyrimidines function specifically through activation of p53.

Through a high-throughput screening effort, chromenotriazolopyrimidine **1** was identified as a novel inhibitor of the MDM2−p53 protein−protein interaction. The fairly rigid chromenotriazolopyrimidine core was shown to be an efficient scaffold from which to project substituents into the key p53 binding pockets of the MDM2 protein. The hit compound was developed into a tractable lead series with clear SAR trends toward improved potency that were largely consistent with cocrystallography data. The cellular mechanism of action was consistent with activation of p53. The discovery and validation of new potent inhibitors such as **23** and **37** is an important step toward testing the hypothesis of p53−MDM2 inhibition in the treatment of cancer.

Experimental Section

Biochemical Assays and Crystallography. Details of the HTRF Screen: Test compounds in 3-fold dilutions were incubated with 0.005 μM N-terminal GST-tagged human MDM2 (1−188) and 0.01 μM Avi-tagged p53 (1−83) with detection by time-resolved fluorescence spectroscopy.

Details of the SPR Direct Binding Assay Using a Biacore T100 Instrument: Human MDM2 (17−125), p53 (1−83), and GST were separately immobilized onto three flow cells of a CM5 chip using amine coupling chemistry. Test compounds in 3-fold dilutions were flowed over the surfaces. K_d values were calculated using curve fitting to the measured binding sensorgrams in Scrubber-2 evaluation software (version 2).

Details of the MDM2 Autoubiquitination Assay: Test compounds in 3-fold dilutions were incubated with human GST−MDM2 immobilized on an electrochemiluminescence plate. ATP, ubiquitin, UBE1, and UbcH5b were combined separately and added to the plate. After 60 min, the reaction was quenched, sulfotag-labeled antiubiquitin antibody was added, and ubiquitination was detected by electrochemiluminescence (Mesoscale Discovery, Gaithersburg, MD). Human MDM2 16−111 was cocrystallized with **1a** in P4$_1$2$_1$2 space-group with $a = b = 34.5$ Å and $c = 161.2$ Å at 2.1 Å resolution (PDB code 3JZK).

Cellular Assays. p53 Dual-Luciferase Reporter Assay: HCT116 cells were stably cotransfected with mammalian expression vectors pp53-TA-Luc (Clontech, Mountain View, CA) and pRL-SV40

(Promega, Madison, WI), and a single clone (HCT116 pp53-TA-Luc) was used in the assay. pp53-TA-Luc contained a p53 response element located upstream of the minimal transcription activation (TA) promoter. Located downstream of the TA promoter was the firefly luciferase reporter gene (*luc*). pRL-SV40 provided constitutive expression of *Renilla* luciferase and was used to normalize firefly luciferase activity. In the assay, HCT116 pp53-TA-Luc cells were seeded at 20 000 cells/well in a 96-well tissue culture plate in growth media (McCoy's 5A with 10% fetal bovine serum) at 37 °C 16 h prior to compound treatment. Compounds were serially diluted in DMSO and added to the cells in growth media at 1% final DMSO concentration. Compound-containing media was removed 8 h post-treatment, and cells were frozen at −80 °C. The firefly and *Renilla* luciferase activities in cell lysates were measured on an LMAXII luminometer (Molecular Devices, Sunnyvale, CA) using the Dual-Luciferase Assay System (Promega, Madison, WI) following the manufacturer's protocol. The reporter activity was calculated as the ratio of firefly and *Renilla* luciferase activities.

Real-Time RT-PCR. HCT116 and HCT116 $p53^{-/-}$[22a] cells were seeded and treated as above. Cells from triplicate wells were harvested and pooled 16 h post-compound treatment. Total RNA was extracted from cell pellets using the RNeasy Mini Kit (Qiagen, Valencia, CA). The expression levels of p21 and GAPDH mRNA were quantified by real-time RT-PCR using primers (Hs00355782_m1 p21 and Hs99999905_m1 GAPDH) and TaqMan One-Step RT-PCR Master Mix Reagents (4309169, Applied Biosystems, Foster City, CA) on an ABI PRISM sequence detector. The expression levels were calculated based on standard curves generated from total RNA, and p21 expression was normalized with GAPDH.

Cell Proliferation Assay: HCT116, HCT116 $p53^{-/-}$,[22a] and HCT116 $p21^{-/-}$[22b] cells were seeded and treated with compounds for 16 h. 5-Bromo-2-deoxyuridine (BrdU) (00-0103, Invitrogen, Carlsbad, CA) was added to the cells 1 h prior to harvest. Cells from triplicate wells were pooled and fixed with ice-cold 90% methanol. The fixed cells were incubated in acid buffer (2 N HCl in 0.5% Triton X-100) for 1 h followed by staining with 3 μg/mL anti-BrdU Alexa 647 (A21305, Invitrogen, Carlsbad, CA) in wash buffer (1% BSA, 0.5% Triton X-100 in phosphate-buffered saline) for 1 h. Cells were stained with propidium iodide (550825, BD Biosciences Pharmingen, San Diego, CA) before analysis using an LSRII flow cytometer (BD Biosciences Pharmingen, San Diego, CA). Inhibition of proliferation was calculated as the percentage of inhibition of BrdU-positive cells compared with DMSO controls.

Apoptosis Assay: SJSA-1 cells (ATCC, Manassas, VA) were seeded and treated with compounds in a 96-well black wall, clear bottom tissue culture plate (3904, Corning, Corning, NY) in growth media (RPMI 1640 media with 10% fetal bovine serum and 1 mM sodium pyruvate) as above. Caspase-3/7 activity was measured 48 h post treatment using Apo-ONE Homogeneous Caspase-3/7 assay kit (G7791, Promega, Madison, WI) following the manufacturer's protocol. Cells were incubated with assay reagents for 2 h at room temperature prior to recording fluorescence (relative fluorescence units $485_{Ex}/538_{Em}$) using a SpectraMax M5 (Molecular Devices, Sunnyvale, CA) fluorescence reader.

Total and Phospho-p53 Assay: HCT116 cells were seeded and treated with compounds in a 96-well imaging plate (BD 353219) as above. Total p53 and phospho-p53 (Ser15) were stained 24 h post-compound treatment using Phospho-p53 and p53 detection kit (5400502, Thermo Scientific, Waltham, MA) following the manufacturer's protocol. Stained cells were evaluated using an ArrayScan V^{TI} (Cellomics, Pittsburgh, PA) instrument and analyzed with Target Activation BioApplication (Thermo Scientific, Waltham, MA) software.

General Chemistry Procedures. Starting materials were commercially available from Aldrich (Milwaukee, WI), Acros Organics (Geel, Belgium), and InterBioScreen (Moscow, Russia). Solvents were anhydrous and were used as received. Column chromatography was performed using silica gel 60 (230−400 mesh), and reaction progress was determined by TLC analysis on Baker Si250F glass plates with visualization under UV light. Melting points were determined using a Buchi melting point B-545 with automatic detection, 1 °C/min heating rate, and are uncorrected. IR spectra were recorded using a Perkin-Elmer Spectrum One FT-IR spectrophotometer and Universal ATR sampling accessory. ^{1}H NMR spectra were recorded using a Bruker DRX-400 (400 MHz) NMR spectrometer. Chemical shifts are given in parts per million (ppm), and TMS was used as an internal standard. All coupling constants (J) are given in Hz (in NMR description, s = singlet, br s = broad singlet, d = doublet, t = triplet, dd = doublet of doublets, m = muliplet). Elemental analyses were used to determine purity >95% and were preformed by Atlantic Microlab (Norcross, GA). In cases where elemental analyses were not run, HPLC was used to determine purity >95%, except for compounds **21**, **23**, and **32**, which had lower purity as reported below. HPLC purity (%) and retention time (RT, min) were determined using an Agilent Technologies 1100 Series HPLC and the following conditions: condition A, Agilent Zorbax XDB C8 150 × 4.6 mm^2 5 μm column with a 1.5 mL/min binary gradient 0−10 min 95:5 to 5:95 water 0.1% TFA/ACN 0.07% TFA; condition B, Phenomix Synergi 4u MAX-RP 50 × 2.00 mm^2 4 μm column with a 1.5 mL/min binary gradient 0−3 min 90:10 to 5:95, 3−3.5 min 5:95 water 0.1% TFA/ACN 0.1% TFA; condition C, Agilent Scalar C18 150 × 4.6 mm^2 5 μm with a 1.5 mL/min binary gradient 0−10 min 95:5−5:95 water 0.1% TFA/ACN 0.07% TFA; condition D, Phenomix Luna C8 100 × 4.6 mm^2 5 μm with a 1.0 mL/min binary gradient 0−0.5 min 90:10, 0.5−13.5 min 90:10 to 0:100, 13.5−14.5 min 0:100 water 0.1% TFA/ACN 0.1% TFA; condition E, Phenomix Synergi 4u MAX-RP 50 × 2.00 mm^2 4 μm column with a 1.5 mL/min binary gradient 0−3 min 90:10 to 5:95, 3−3.5 min 5:95 water 0.1% formic acid/ACN 0.1% formic acid. ESI (electrospray ionization) mass spectra were recorded using an Agilent Technologies 1100 Series HPLC and LC/MSD SL mass spectrometer. ESI (electrospray ionization) high-resolution mass spectra were recorded using an Agilent Technologies 1200 Series HPLC and LC/MSD TOF mass spectrometer.

Representative Synthesis of 11 According to Scheme 2 (Method A). (2*E*)-3-(4-Bromophenyl)-1-(2-hydroxyphenyl)prop-2-en-1-one (5, R^1 = Br, R^3 = H): Potassium hydroxide (27.0 g, 0.48 mol) was stirred in ethanol (95%, 200 mL) until complete dissolution of the hydroxide occurred. 1-(2-Hydroxyphenyl)ethanone (16.4 mL, 0.135 mol) was added with a small amount of ethanol (yellow solids formed) followed after 5 min by 4-bromobenzaldehyde (25.0 g, 0.13 mol), at which point the reaction mixture became a clear red solution with some solids remaining (slightly exothermic). After 15−20 min, the reaction mixture became a very thick red-orange mass. The reaction mixture was stirred at room temperature overnight. The reaction mixture was poured into 1.2 L of ice water, and the reaction flask was rinsed with water. The mixture was stirred for 30 min to mix completely, and then 130 mL of concentrated hydrochloric acid was added. After 2 h, the mixture was filtered on a Büchner funnel, washing with water. The dried cake was dissolved in 1 L of methylene chloride, the aqueous layer was drawn off, and the organic layer was dried over sodium sulfate. The solvent was evaporated *in vacuo* to afford the title compound (37.1 g, 91%) as a yellow solid that was used directly in the next step, mp 140.6 °C: IR (neat) cm^{-1} 2818, 1641, 1562, 1485, 1178, 982, 745; ^{1}H NMR (400 MHz, DMSO-d_6) δ ppm 12.42 (s, 1 H), 8.23−8.26 (m, 1 H), 8.07 (d, J = 15.4 Hz, 1 H), 7.78−7.90 (m, 3 H), 7.68 (ddd, J = 8.7, 2.4, 2.1 Hz, 2 H), 7.57 (ddd, J = 8.4, 7.1, 1.7 Hz, 1 H), 6.98−7.03 (m, 2 H); MS (ESI+) m/z 303.0 $(M + H)^+$; Anal. ($C_{15}H_{12}BrO_2$) C, H.

(±)-2-[7-(4-Bromophenyl)-4,7-dihydro[1,2,4]triazolo[1,5-*a*]-pyrimidin-5-yl]phenol (6, R^1 = Br, R^3 = H): To (2*E*)-3-(4-bromophenyl)-1-(2-hydroxyphenyl)prop-2-en-1-one (26.6 g, 87.6 mmol) was added 3-amino-1,2,4-triazole (7.75 g, 87.6 mmol).

The neat reaction mixture was heated to 165 °C until the material solidified (20−30 min). The reaction mixture was cooled to room temperature to provide a reddish orange solid glassy material. Chloroform (300 mL) was added, and the solid was broken up with a spatula. The mixture was stirred for 2−3 h and then filtered, washing with chloroform (100 mL). The solvent was removed *in vacuo* to afford the title compound as a yellow solid (32.3 g, 94%), mp 173.8 °C: IR (neat) cm^{-1} 3337, 2580, 1587, 1456, 1242, 1195, 1011, 841; ^1H NMR (400 MHz, DMSO-d_6) δ ppm 7.37−7.43 (m, 4 H), 7.11 (ddd, J = 8.2, 4.5, 2.0 Hz, 3 H), 7.02 (td, J = 7.7, 1.6 Hz, 1.0 H), 6.72 (s, 1 H), 6.71 (d, J = 1.0 Hz, 1 H), 6.64 (td, J = 7.5, 1.1 Hz, 1 H), 6.02 (d, J = 3.5 Hz, 1 H), 4.74 (d, J = 3.7 Hz, 1 H); MS (ESI+) m/z 369.0 $(M + H)^+$; Anal. ($C_{17}H_{14}BrN_4O$) C, H, N.

(±)-6,7-Bis(4-bromophenyl)-7,12-dihydro-6*H*-chromeno[4,3-*d*][1,2,4]triazolo[1,5-*a*]pyrimidine (1 or 7, $R^1 = R^2 = Br$, $R^3 = H$): (±)-2-[7-(4-Bromophenyl)-4,7-dihydro[1,2,4]triazolo[1,5-*a*]-pyrimidin-5-yl]phenol (12.2 g, 33.1 mmol) and 4-bromobenzaldehyde (8.2 g, 4.4 mmol) were mixed together neat and then heated with stirring at 160 °C for 30 min until the reaction mixture solidified. The reaction mixture was cooled to room temperature, and chloroform (60 mL) was added. The reaction mixture was stirred for 1 h, and the mixture was filtered on a Büchner funnel, washing with chloroform (150 mL). The title compound was obtained as a pale yellow solid mixture of *syn* and *anti* stereoisomers (1:5 *syn*/*anti*, 6.16 g, 34%), mp 240.9 °C: IR (neat) cm^{-1} 3046, 1656, 1552, 1486, 1236, 1010, 819, 759; *anti* isomer ^1H NMR (400 MHz, DMSO-d_6) δ ppm 10.55 (s, 1 H), 7.82 (dd, J = 7.8, 1.2 Hz, 1 H), 7.67−7.69 (m, 1 H), 7.53−7.62 (m, 4 H), 7.33 (d, J = 8.4 Hz, 2 H), 7.21−7.26 (m, 3 H), 7.00−7.05 (m, 1 H), 6.77 (d, J = 7.2 Hz, 1 H), 5.73 (s, 1 H), 5.40 (s, 1 H); *syn* isomer ^1H NMR (400 MHz, DMSO-d_6) δ ppm 7.80 (d, J = 7.6 Hz, 1 H), 7.68−7.70 (m, 1 H), 7.20 (dd, J = 15.5, 1.3 Hz, 1 H), 7.13 (dd, J = 8.4, 2.1 Hz, 4 H), 7.02 (t, J = 7.2 Hz, 1 H), 6.81 (d, J = 8.2 Hz, 4 H), 6.72 (d, J = 8.0 Hz, 1 H), 5.87 (s, 1 H), 6.18 (s, 1 H); HPLC condition A: 5.28, 5.64 min, 1:5 ratio; MS (ESI+) m/z 535.0 $(M + H)^+$; Anal. ($C_{24}H_{17}Br_2N_4O$) C, H, N.

(±)-*syn*-6,7-Bis(4-bromophenyl)-12-methyl-7,12-dihydro-6*H*-chromeno[4,3-*d*][1,2,4]triazolo[1,5-*a*]pyrimidine, 11: (±)-6,7-Bis-(4-bromophenyl)-7,12-dihydro-6*H*-chromeno[4,3-*d*][1,2,4]triazolo[1,5-*a*]pyrimidine (856 mg, 1.6 mmol), cesium carbonate (1.0 g, 3.2 mmol), and methyl iodide (0.2 mL, 3.0 mmol) were stirred at room temperature for 30 min. The reaction was quenched with water, and a white solid precipitate was observed. The mixture was filtered, and the solid was dried under high vacuum. The residue was purified by chromatography on silica gel, eluting with ethyl acetate−hexane gradient (1:19−2:3 ethyl acetate−hexane) to give the *syn* product as a clear glass. Ether was added, and the white solid that resulted was filtered to provide the title compound (0.50 g, 57%), mp 152.5 °C: IR (neat) cm^{-1} 3681, 2982, 1635, 1553, 1070, 764; ^1H NMR (400 MHz, DMSO-d_6) δ ppm 7.74 (s, 1 H), 7.66 (d, J = 7.9 Hz, 1 H), 7.24 (t, J = 7.7 Hz, 1 H), 7.20−7.07 (m, 5 H), 6.82 (t, J = 8.9 Hz, 5 H), 6.09 (s, 1 H), 5.81 (s, 1 H), 3.53 (s, 3 H); MS (ESI+) m/z 549.0 $(M + H)^+$; Anal. ($C_{25}H_{19}Br_2N_4O$) C, H, N.

Representative Synthesis of 11 According to Scheme 3 (Method B). (±)-7-(4-Bromophenyl)-5-(2-{[*tert*-butyl(dimethyl)silyl]oxy}-phenyl)-4,7-dihydro[1,2,4]triazolo[1,5-*a*]pyrimidine: (±)-2-[7-(4-Bromophenyl)-4,7-dihydro[1,2,4]triazolo[1,5-*a*]pyrimidin-5-yl]-phenol (**6**, R^1 = Br, R^3 = H; 5.00 g, 13.5 mmol) was taken up in methylene chloride (36 mL), and triethylamine (9.0 mL, 64.0 mmol) was added to the slurry, followed by *tert*-butyldimethylsilyl chloride (2.88 g, 19.1 mmol) in one portion. The reaction mixture was stirred under nitrogen 16 h. The solvent was removed *in vacuo* to yield a white solid. The solid was triturated with a mixture of 150 mL of hexanes/15 mL of ethyl acetate, and the solids were filtered off. The solid was suspended in methylene chloride (20 mL) and purified by chromatography on silica gel, eluting with a gradient of hexanes to 9:1 ethyl acetate−hexanes to provide the product as a white solid (5.33 g, 81%): ^1H NMR (400 MHz, chloroform-*d*) δ ppm 8.62 (s, 1 H), 7.20−7.33 (m, 5 H), 7.03−7.12 (m, 4 H), 6.83 (s, 1 H), 6.81 (d, J = 1.0 Hz, 1 H), 6.71 (dd, J = 8.1, 0.88 Hz, 1 H), 5.96 (d, J = 3.5 Hz, 1 H), 4.79 (dd, J = 3.5, 1.8 Hz, 1 H), 0.75 (s, 10 H), −0.18 (s, 2 H); HPLC condition A, 5.97 min, 97.5% 210 nm, 97.2% 250 nm; condition B, 3.51 min, 100% 215 nm, 100% 254 nm; HRMS calcd for $C_{23}H_{26}BrN_4OSi$ 483.1210, found 483.1193.

(±)-7-(4-Bromophenyl)-5-(2-{[*tert*-butyl-(dimethyl)silyl]oxy}phenyl)-4-methyl-4,7-dihydro[1,2,4]triazolo-[1,5-*a*]pyrimidine: (±)-7-(4-Bromophenyl)-5-(2-{[*tert*-butyl(dimethyl)silyl]oxy}phenyl)-4,7-dihydro[1,2,4]triazolo[1,5-*a*]pyrimidine (2.60 g, 5.38 mmol) was taken up in 20 mL of dry tetrahydrofuran, and the slurry was cooled to 0 °C. Sodium hydride (165.2 mg, 6.88 mmol, 60% dispersion in mineral oil) was added to the mixture slowly over 1−2 min. After 30 min, methyl iodide (0.38 mL, 6.10 mmol) was added dropwise via syringe over a period of 2 min. The mixture was allowed to warm slowly to room temperature over 3 h. The reaction was quenched by the addition of 40 mL of saturated aqueous ammonium chloride and 75 mL of water. The mixture was extracted with ether (2 × 50 mL), and the combined organic layers were washed with water (2 × 50 mL). The organic layer was dried over sodium sulfate, the reaction mixture was filtered, and the solvent was removed in vacuo to afford the title compound as a yellow pasty residue (2.68 g, 100%). The product was used directly in the next reaction without further purification, mp 152.9 °C: IR (neat) cm^{-1} 2930, 2858, 1568, 1255, 917, 824, 778; ^1H NMR (400 MHz, chloroform-*d*) δ ppm 7.62 (s, 1 H), 7.48 (dd, J = 19.7, 8.5 Hz, 2 H), 7.18−7.34 (m, 4 H), 6.98 (t, J = 7.3 Hz, 1 H), 6.88 (d, J = 0.8 Hz, 1 H), 6.11 (s, 1 H), 4.74 (d, J = 3.5 Hz, 1 H), 3.12−3.18 (m, 3 H), 0.86−0.94 (m, 9 H), 0.10−0.27 (m, 6 H); MS (ESI+) m/z 497.0 $(M + H)^+$; Anal. ($C_{24}H_{30}BrN_4OSi$) C, H, N.

(±)-2-[7-(4-Bromophenyl)-4-methyl-4,7-dihydro[1,2,4]triazolo[1,5-*a*]pyrimidin-5-yl]phenol: (±)-7-(4-Bromophenyl)-5-(2-{[*tert*-butyl(dimethyl)silyl]oxy}phenyl)-4-methyl-4,7-dihydro-[1,2,4]triazolo[1,5-*a*]pyrimidine (2.68 g, 5.0 mmol) was taken up in dimethylformamide/water mixture (10:1, 33 mL), cesium carbonate (886 mg, 3.0 mmol) was added, and the mixture was stirred at room temperature for 1 h. The pH was adjusted to ca. 4 (hydrochloric acid, 6 N), and the mixture was extracted with ether (3 × 75 mL). The combined organic layers were washed with water (4 × 10 mL). The organic layer was dried over sodium sulfate, the mixture was filtered, and the solvent was removed *in vacuo* to afford crude product (2.32 g) as a waxy yellow solid. The solid was triturated with methylene chloride (10 mL) to afford the title compound as a pale yellow solid (0.96 g, 46%), mp 217.6 °C: IR (neat) cm^{-1} 3681, 2950, 1568, 1254, 823, 777; ^1H NMR (400 MHz, DMSO-d_6) δ ppm 9.91 (s, 1 H), 7.66 (s, 1 H), 7.58 (d, J = 8.3 Hz, 2 H), 7.25−7.36 (m, 3 H), 7.18 (d, J = 7.3 Hz, 1 H), 6.92 (d, J = 8.1 Hz, 1 H), 6.83−6.89 (m, 1 H), 6.14−6.24 (m, 1 H), 4.74 (br. s., 1 H), 3.04 (s, 3 H); MS (ESI+) m/z 383.0 $(M + H)^+$; Anal. ($C_{18}H_{16}BrN_4O$) C, H, N.

(±)-*syn*-6,7-Bis(4-bromophenyl)-12-methyl-7,12-dihydro-6*H*-chromeno[4,3-*d*][1,2,4]triazolo[1,5-*a*]pyrimidine (11): (±)-2-[7-(4-Bromophenyl)-4-methyl-4,7-dihydro[1,2,4]triazolo[1,5-*a*]pyrimidin-5-yl]phenol (205 mg, 0.535 mmol), dry dimethylformamide (1.5 mL), 1-bromo-4-(dimethoxymethyl)benzene (0.50 mL, 3.0 mmol), samarium(III) trifluoromethanesulfonate (214 mg, 0.358 mmol), and trifluoroacetic acid (0.10 mL, 1.3 mmol) were combined and warmed 3 h at 70 °C. The mixture was diluted with diethyl ether (50 mL) and washed with water (4 × 5 mL), aqueous sodium bicarbonate (1 × 5 mL), and water (3 × 5 mL). The organic layer was dried over sodium sulfate and filtered, and the solvent was removed *in vacuo* giving a near colorless oil (0.8 g). Purification by chromatography on silica gel eluting with a gradient of 9:1 acetate/hexane to ethyl acetate gave the title compound as a white solid (233 mg, 79% yield). Characterization data was consistent with **11** prepared by method A.

SAR Compounds. Yields were given for the racemic *syn* product and were based on **7** for compounds prepared by method A or **36** for compounds prepared by method B.

(±)-***syn*-6,7-Bis(4-fluorophenyl)-12-methyl-7,12-dihydro-6*H*-chromeno[4,3-*d*][1,2,4]triazolo[1,5-*a*]pyrimidine, 9:** Method A (40%), mp 187.8 °C: IR (neat) cm^{-1} 2925, 1727, 1644, 1506, 1420, 1221, 1041, 837, 769; ^1H NMR (400 MHz, chloroform-*d*) δ ppm 7.67 (s, 1 H), 7.54 (dd, *J* = 7.9, 1.7 Hz, 1 H), 7.31−7.24 (m, 2 H), 7.16−7.10 (m, 1 H), 6.96−6.84 (m, 4 H), 6.79−6.67 (m, 4 H), 5.82 (s, 1 H), 5.60 (s, 1 H), 3.66 (s, 3 H); MS (ESI+) *m*/*z* 429.0 $(M + H)^+$; Anal. ($C_{25}H_{19}F_2N_4O$) C, H, N.

(±)-***syn*-6,7-Bis(4-chlorophenyl)-12-methyl-7,12-dihydro-6*H*-chromeno[4,3-*d*][1,2,4]triazolo[1,5-*a*]pyrimidine, 10:** Method A (77%), mp 144.6 °C: IR (neat) cm^{-1} 2923, 1634, 1558, 1486, 173, 1010, 831; ^1H NMR (400 MHz, chloroform-*d*) δ ppm 7.66 (s, 1 H), 7.54 (dd, *J* = 7.9, 1.7 Hz, 1 H), 7.24−7.32 (m, 2 H), 7.13 (t, *J* = 7.5 Hz, 1 H), 6.96−7.06 (m, 4 H), 6.93 (d, *J* = 7.0 Hz, 1 H), 6.78−6.89 (m, 3 H), 5.81 (s, 1 H), 5.58 (s, 1 H), 3.66 (s, 3 H); MS (ESI+) *m*/*z* 460.9 $(M + H)^+$; Anal. ($C_{25}H_{19}Cl_2N_4O$) C, H, N.

(±)-***syn*-7-(4-Bromophenyl)-6-(4-fluorophenyl)-12-methyl-7,12-dihydro-6*H*-chromeno[4,3-*d*][1,2,4]triazolo[1,5-*a*]pyrimidine, 12:** Method B (50%), mp 179.2 °C: IR (neat) cm^{-1} 2916, 1639, 1559, 1485, 1213, 1010, 815, 730; ^1H NMR (400 MHz, DMSO-d_6) δ ppm 7.73 (s, 1 H), 7.66 (d, *J* = 7.9 Hz, 1 H), 7.24 (t, *J* = 8.5 Hz, 1 H), 7.17 (d, *J* = 8.3 Hz, 2 H), 7.11 (t, *J* = 7.6 Hz, 1 H), 6.89−6.95 (m, 2 H), 6.81−6.87 (m, 3 H), 6.73−6.80 (m, 2 H), 6.08 (s, 1 H), 5.83 (s, 1 H), 3.53 (s, 3 H); MS (ESI+) *m*/*z* 488.9 $(M + H)^+$; Anal. ($C_{25}H_{18}BrFN_4O \cdot H_2O$) C, H, N.

(±)-***syn*-7-(4-Bromophenyl)-6-(4-chlorophenyl)-12-methyl-7,12-dihydro-6*H*-chromeno[4,3-*d*][1,2,4]triazolo[1,5-*a*]pyrimidine, 13:** Method A (8%), mp 177.8 °C: IR (neat) cm^{-1} 2922, 1643, 1559, 1487, 1410, 1213, 1073, 967, 833; ^1H NMR (400 MHz, DMSO-d_6) δ ppm 7.74 (s, 1 H), 7.64−7.69 (m, 1 H), 7.21−7.27 (m, 1 H), 7.17 (d, *J* = 8.3 Hz, 2 H), 7.08−7.14 (m, 1 H), 7.00 (d, *J* = 8.5 Hz, 2 H), 6.80−6.91 (m, 5 H), 6.09 (s, 1 H), 5.83 (s, 1 H), 3.53 (s, 3 H); HPLC condition A, 7.46 min, 97.7% 210 nm, 99.3% 254 nm; HRMS calcd for $C_{25}H_{19}BrClN_4O$ 505.0425, found 505.0413.

(±)-***syn*-7-(4-Bromophenyl)-12-methyl-6-(4-methylphenyl)-7,12-dihydro-6*H*-chromeno[4,3-*d*][1,2,4]triazolo[1,5-*a*]pyrimidine, 14:** Method B (10%), mp 159.9 °C: IR (neat) cm^{-1} 2926, 1638, 1557, 1484, 1406, 1174, 1010, 816, 730; ^1H NMR (400 MHz, DMSO-d_6) δ ppm 7.73 (s, 1 H), 7.65 (d, *J* = 7.7 Hz, 2 H), 7.22 (t, *J* = 7.7 Hz, 1 H), 7.17−7.06 (m, 3 H), 6.85−6.76 (m, 3 H), 6.74 (s, 4 H), 6.06 (s, 1 H), 5.75 (s, 1 H), 3.53 (s, 3 H), 2.14 (s, 3 H); MS (ESI+) *m*/*z* 484.9 $(M + H)^+$; Anal. ($C_{26}H_{22}BrN_4O$) C, H, N.

(±)-***syn*-4-[6-(4-Bromophenyl)-12-methyl-7,12-dihydro-6*H*-chromeno[4,3-*d*][1,2,4]triazolo[1,5-*a*]pyrimidin-7-yl]benzonitrile, 15:** Method B (32%), mp 183.8 °C: IR (neat) cm^{-1} 2923, 1656, 1555, 1454, 1234, 1072, 1011, 821, 762; ^1H NMR (400 MHz, DMSO-d_6) δ ppm 7.76 (s, 1 H), 7.67 (d, *J* = 7.9 Hz, 1 H), 7.45 (d, *J* = 8.1 Hz, 2 H), 7.25 (t, *J* = 7.8 Hz, 1 H), 7.11 (t, *J* = 9.0 Hz, 5 H), 6.81 (d, *J* = 8.3 Hz, 2 H), 6.84 (d, *J* = 8.1 Hz, 1 H), 6.22 (s, 1 H), 5.85 (s, 1 H), 3.55 (s, 3 H); MS (ESI+) *m*/*z* 496.0 $(M + H)^+$; Anal. ($C_{26}H_{19}BrN_5O \cdot H_2O$) C, H, N.

(±)-***syn*-7-(4-Bromophenyl)-6-(4-ethynylphenyl)-12-methyl-7,12-dihydro-6*H*-chromeno[4,3-*d*][1,2,4]triazolo[1,5-*a*]pyrimidine, 16:** Method B (22%), mp 109.5 °C: IR (neat) cm^{-1} 2922, 1634, 1558, 1486, 1408, 1173, 1071, 1010, 829; ^1H NMR (400 MHz, DMSO-d_6) δ ppm 7.74 (s, 1 H), 7.67 (d, *J* = 7.9 Hz, 1 H), 7.23 (t, *J* = 7.7 Hz, 1 H), 7.15 (d, *J* = 8.5 Hz, 1 H), 7.11 (t, *J* = 7.0 Hz, 1 H), 7.04 (d, *J* = 8.3 Hz, 2 H), 6.90−6.81 (m, 5 H), 6.09 (s, 1 H), 5.83 (s, 1 H), 4.14 (s, 1 H), 3.53 (s, 3 H); MS (ESI+) *m*/*z* 494.9 $(M + H)^+$; Anal. ($C_{27}H_{20}BrN_4O \cdot 2H_2O$) C, H, N.

(±)-***syn*-7-(4-Bromophenyl)-12-methyl-6-(4-prop-1-yn-1-ylphenyl)-7,12-dihydro-6*H*-chromeno[4,3-*d*][1,2,4]triazolo[1,5-*a*]pyrimidine, 17:** Method B (13%), mp 180.6 °C: IR (neat) cm^{-1} 2915, 1631, 1560, 1485, 1407, 1174, 1070, 822; ^1H NMR (400 MHz, DMSO-d_6) δ ppm 7.73 (s, 1 H), 7.66 (d, *J* = 7.9 Hz, 2 H), 7.23 (s, 1 H), 7.16 (d, *J* = 8.3 Hz, 2 H), 7.11 (d, *J* = 7.7 Hz, 1 H), 6.91−6.98 (m, 2 H), 6.83 (dd, *J* = 8.4, 2.2 Hz, 4 H), 6.08 (s, 1 H), 5.80 (s, 1 H), 3.53 (s, 3 H), 1.99 (s, 3 H); MS (ESI+) *m*/*z* 508.9 $(M + H)^+$; Anal. ($C_{28}H_{22}BrN_4O$) C, H, N.

(±)-***syn*-7-(4-Bromophenyl)-6-(4-ethylphenyl)-12-methyl-7,12-dihydro-6*H*-chromeno[4,3-*d*][1,2,4]triazolo[1,5-*a*]pyrimidine, 18:** Method B (30%), mp 163.3 °C: IR (neat) cm^{-1} 2822, 1640, 1561, 1485, 1203, 1007, 814, 668; ^1H NMR (400 MHz, DMSO-d_6) δ ppm 7.72 (s, 1 H), 7.65 (d, *J* = 7.7 Hz, 1 H), 6.72−7.27 (m, 11 H), 6.05 (s, 1 H), 5.75 (s, 1 H), 3.53 (s, 3 H), 2.42 (q, *J* = 7.5 Hz, 2 H), 1.09 (t, *J* = 7.6 Hz, 3 H); MS (ESI+) *m*/*z* 499.0 $(M + H)^+$; Anal. ($C_{27}H_{24}BrN_4O \cdot H_2O$) C, H, N.

(±)-***syn*-6-(4-Bromophenyl)-7-(4-fluorophenyl)-12-methyl-7,12-dihydro-6*H*-chromeno[4,3-*d*][1,2,4]triazolo[1,5-*a*]pyrimidine, 19:** Method B (36%), mp 171.4 °C: IR (neat) cm^{-1} 3044, 1655, 1552, 1454, 1236, 1071, 1010, 821; ^1H NMR (400 MHz, DMSO-d_6) δ ppm 7.73 (s, 1 H), 7.66 (d, *J* = 7.9 Hz, 1 H), 7.27−7.21 (m, 1 H), 7.17−7.08 (m, 3 H), 6.96−6.90 (m, 2 H), 6.87−6.76 (m, 5 H), 6.10 (s, 1 H), 5.83 (s, 1 H), 3.53 (s, 3 H); MS (ESI+) *m*/*z* 488.8 $(M + H)^+$; Anal. ($C_{25}H_{19}BrFN_4O$) C, H, N.

(±)-***syn*-6-(4-Bromophenyl)-12-methyl-7-(4-methylphenyl)-7,12-dihydro-6*H*-chromeno[4,3-*d*][1,2,4]triazolo[1,5-*a*]pyrimidine, 20:** Method B (10%), mp 160.5 °C: IR (neat) cm^{-1} 1641, 1558, 1415, 1215, 1010, 816, 750; ^1H NMR (400 MHz, DMSO-d_6) δ ppm 7.71 (s, 1 H), 7.65 (d, *J* = 7.9 Hz, 1 H), 7.23 (t, *J* = 7.8 Hz, 1 H), 7.13−7.07 (m, 3 H), 6.84 (d, *J* = 8.1 Hz, 1 H), 6.81−6.75 (m, 4 H), 6.74−6.69 (m, 2 H), 5.99 (s, 1 H), 5.80 (s, 1 H), 3.53 (s, 3 H), 2.11 (s, 3 H); MS (ESI+) *m*/*z* = 484.7 $(M + H)^+$; Anal. ($C_{26}H_{22}BrN_4O$) C, H, N.

(±)-***syn*-4-[6-(4-Bromophenyl)-12-methyl-7,12-dihydro-6*H*-chromeno[4,3-*d*][1,2,4]triazolo[1,5-*a*]pyrimidin-7-yl]benzonitrile, 21:** Method B (28%); ^1H NMR (400 MHz, DMSO-d_6) δ ppm 7.76 (s, 1 H), 7.67 (d, *J* = 8.5 Hz, 1 H), 7.45 (d, *J* = 7.7 Hz, 2 H), 7.29−7.21 (m, 1 H), 7.11 (t, *J* = 8.60 Hz, 5 H), 6.88−6.77 (m, 3 H), 6.22 (s, 1 H), 5.85 (s, 1 H), 3.55 (s, 3 H); HPLC condition C, 4.93 min, 94.6% 210 nm, 94.3%, 250 nm; HRMS calcd for $C_{26}H_{19}BrN_5O$ 496.0767, found 496.0691.

(±)-***syn*-6,7-Bis(4-bromophenyl)-1-fluoro-12-methyl-7,12-dihydro-6*H*-chromeno[4,3-*d*][1,2,4]triazolo[1,5-*a*]pyrimidine, 22:** Method A (28%), mp 158.2 °C: IR (neat) cm^{-1} 1639, 1460, 1253, 1171, 1009, 785, 765, 725; ^1H NMR (400 MHz, DMSO-d_6) δ ppm 7.77 (s, 1 H), 7.23−7.33 (m, 1 H), 7.12−7.23 (m, 4 H), 6.95−7.02 (m, 1 H), 6.92 (d, 2 H), 6.80 (d, 2 H), 6.72 (d, 1 H), 6.20 (s, 1 H), 5.86 (s, 1 H), 3.34 (s, 3 H); MS (ES+) *m*/*z*: 568.9 $(M + H)^+$; Anal. ($C_{25}H_{18}Br_2FN_4O$) C, H, N.

(±)-***syn*-6,7-Bis(4-bromophenyl)-12-methyl-1-(methyloxy)-7,12-dihydro-6*H*-chromeno[4,3-*d*][1,2,4]triazolo[1,5-*a*]pyrimidine, 23:** Method B (13%): ^1H NMR (400 MHz, DMSO-d_6) δ ppm 7.74 (s, 1 H), 7.30−7.09 (m, 5 H), 6.91 (d, *J* = 8.3 Hz, 2 H), 6.82−6.72 (m, 3 H), 6.46 (d, *J* = 8.1 Hz, 1 H), 6.17 (s, 1 H), 5.74 (s, 1 H), 3.92 (s, 3 H), 3.25 (s, 3 H); HPLC condition C, 5.42 min, 100% 210 nm, 100% 250 nm; HPLC condition E, 2.73 min, 88% 215 nm, 94% 254 nm; MS (ESI+) for $C_{26}H_{20}Br_2N_4O_2$ *m*/*z* = 578.8 $(M + H)^+$.

(±)-***syn*-6,7-Bis(4-bromophenyl)-1-ethoxy-12-methyl-7,12-dihydro-6*H*-chromeno[4,3-*d*][1,2,4]triazolo[1,5-*a*]pyrimidine, 24:** Method B (12%): IR (neat) cm^{-1} 2922, 1632, 1555, 1458, 1256, 1067, 1009, 877, 722; ^1H NMR (400 MHz, DMSO-d_6) δ ppm 7.71 (s, 1 H), 7.07−7.32 (m, 5 H), 6.70−6.96 (m, 5 H), 6.48 (d, *J* = 7.9 Hz, 1 H), 6.11 (br. s., 1 H), 5.71 (s, 1 H), 4.03−4.32 (m, 2 H), 3.27 (s, 3 H), 1.41 (t, *J* = 6.8 Hz, 3 H); HPLC condition A but with a 12 min gradient, 5.67 min, 100% 210 nm, 100% 250 nm; condition B, 2.84 min, 100% 215 nm, 100% 254 nm; MS (ESI+) for $C_{27}H_{22}Br_2N_4O_2$ *m*/*z* 592.8 $(M + H)^+$.

(±)-***syn*-6,7-Bis(4-bromophenyl)-2-fluoro-12-methyl-7,12-dihydro-6*H*-chromeno[4,3-*d*][1,2,4]triazolo[1,5-*a*]pyrimidine, 25:** Method B (10%), mp 199.7 °C: IR (neat) cm^{-1} 2923, 1644, 1560, 1485, 1408, 992, 736; ^1H NMR (400 MHz, DMSO-d_6) δ ppm 7.74 (s, 1 H), 7.55−7.48 (m, 1 H), 7.20−7.05 (m, 5 H), 6.89−6.77 (m, 5 H), 6.11 (s, 1 H), 5.82 (s, 1 H), 3.54 (s, 3 H); MS (ESI+) *m*/*z* 556.9 $(M + H)^+$; Anal. ($C_{25}H_{18}Br_2FN_4O \cdot H_2O$) C, H, N.

(±)-*syn*-6,7-Bis(4-bromophenyl)-2-chloro-12-methyl-7,12-dihydro-6*H*-chromeno[4,3-*d*][1,2,4]triazolo[1,5-*a*]pyrimidine, 26: Method B (7%): ^{1}H NMR (400 MHz, DMSO-d_6) δ ppm 7.75 (s, 1 H), 7.70−7.66 (m, 1 H), 7.31−7.26 (m, 1 H), 7.16 (t, J = 7.6 Hz, 4 H), 6.89−6.78 (m, 5 H), 6.13 (s, 1 H), 5.86 (s, 1 H), 3.54 (s, 3 H); HPLC condition C, 6.00 min, 100% 210 nm, 100% 250 nm; condition B, 2.96 min, 96% 215 nm, 97% 254 nm; HRMS calcd for $C_{25}H_{18}Br_2ClN_4O$ 582.9530, found 582.9317.

(±)-*syn*-6,7-Bis(4-bromophenyl)-2,12-dimethyl-7,12-dihydro-6*H*-chromeno[4,3-*d*][1,2,4]triazolo[1,5-*a*]pyrimidine, 27: Method B (20%): ^{1}H NMR (400 MHz, DMSO-d_6) δ ppm 7.74 (s, 1 H), 7.46 (s, 1 H), 7.14 (dd, J = 13.9, 8.3 Hz, 4 H), 7.03 (d, J = 8.1 Hz, 1 H), 6.81 (dd, J = 10.2, 8.5 Hz, 4 H), 6.72 (d, J = 8.3 Hz, 1 H), 6.08 (s, 1 H), 5.76 (s, 1 H), 3.54 (s, 3 H), 2.32 (s, 3 H); HPLC condition A, 7.44 min, 100% 210 nm, 100% 250 nm; HRMS calcd for $C_{26}H_{21}Br_2N_4O$ 563.0077, found 562.9874.

(±)-6,7-Bis(4-bromophenyl)-2-ethyl-12-methyl-7,12-dihydro-6*H*-chromeno[4,3-*d*][1,2,4]triazolo[1,5-*a*]pyrimidine (1:3 *anti*/*syn*), 28: Method B (33%): ^{1}H NMR (400 MHz, DMSO-d_6) δ ppm 7.78 (s, 1 H), 7.73 (s, 1 H), 7.60 (d, J = 8.3 Hz, 1 H), 7.51 (d, J = 8.5 Hz, 1 H), 7.40 (s, 1 H), 7.28 (d, J = 10.0 Hz, 3 H), 7.15 (dd, J = 14.4, 8.4 Hz, 1 H), 7.10−7.03 (m, 1 H), 6.85−6.79 (m, 1 H), 6.77−6.70 (m, 1 H), 5.87 (s, 1 H), 5.78 (s, 1 H), 5.37 (s, 1 H), 3.60−3.52 (m, 3 H), 2.65−2.56 (m, 2 H), 1.22−1.13 (m, 3 H); HPLC condition C, 6.02, 6.15 min, 1:3 ratio; HRMS calcd for $C_{27}H_{23}Br_2N_4O$ 577.0233, found 577.0235.

(±)-*syn*-6,7-Bis(4-bromophenyl)-2-cyano-12-methyl-7,12-dihydro-6*H*-chromeno[4,3-*d*][1,2,4]triazolo[1,5-*a*]pyrimidine, 29: Method A (4%), mp 189.2 °C: IR (neat) cm^{-1} 2923, 2220, 1589, 1454, 1238, 1011, 821, 730; ^{1}H NMR (300 MHz, DMSO-d_6) δ ppm 8.13 (d, J = 1.3 Hz, 1 H), 7.75 (s, 1 H), 7.70 (dd, J = 8.4, 1.5 Hz, 1 H), 7.16 (dd, J = 8.3, 3.1 Hz, 4 H), 7.01 (d, J = 8.3 Hz, 1 H), 6.83 (t, J = 7.8 Hz, 4 H), 6.13 (s, 1 H), 5.98 (s, 1 H), 3.55 (s, 3 H); MS (ESI+) m/z 575.8 (M + H)$^+$; Anal. ($C_{26}H_{18}Br_2N_5O$) C, H, N.

(±)-*syn*-6,7-Bis(4-bromophenyl)-3-fluoro-12-methyl-7,12-dihydro-6*H*-chromeno[4,3-*d*][1,2,4]triazolo[1,5-*a*]pyrimidine, 30: Method B (3%): ^{1}H NMR (400 MHz, DMSO-d_6) δ ppm 7.79 (s, 1 H), 7.16 (dd, J = 8.4, 5.9 Hz, 1 H), 7.00−6.91 (m, 5 H), 6.87−6.75 (m, 5 H), 6.09 (s, 1 H), 5.87 (s, 1 H), 3.52 (s, 3 H); HPLC condition A, 7.31 min, 100% 210 nm, 100% 250 nm; HRMS calcd for $C_{25}H_{18}Br_2FN_4O$ 566.9826, found 566.9626.

(±)-*syn*-6,7-Bis(4-bromophenyl)-3-chloro-12-methyl-7,12-dihydro-6*H*-chromeno[4,3-*d*][1,2,4]triazolo[1,5-*a*]pyrimidine, 31: Method B (4%): ^{1}H NMR (400 MHz, DMSO-d_6) δ ppm 7.75 (s, 1 H), 7.69 (d, J = 8.5 Hz, 1 H), 7.18−7.12 (m, 5 H), 6.98−6.95 (m, 1 H), 6.83 (dd, J = 14.8, 8.0 Hz, 4 H), 6.11 (s, 1 H), 5.88 (s, 1 H), 3.52 (s, 3 H); HPLC condition C, 6.00 min, 100% 210 nm, 100% 250 nm; HRMS calcd for $C_{25}H_{18}Br_2ClN_4O$ 582.9530, found 582.9359.

(±)-*syn*-6,7-Bis(4-bromophenyl)-4-chloro-12-methyl-7,12-dihydro-6*H*-chromeno[4,3-*d*][1,2,4]triazolo[1,5-*a*]pyrimidine, 32: Method B (14%): ^{1}H NMR (400 MHz, MeOH-d_4) δ ppm 7.77 (s, 1 H), 7.57 (dd, J = 7.9, 1.3 Hz, 1 H), 7.34 (dd, J = 8.2, 1.4 Hz, 1 H), 7.09−7.22 (m, 5 H), 6.87 (dd, J = 8.3, 1.5 Hz, 4 H), 6.06 (s, 1 H), 5.81 (s, 1 H), 3.60 (s, 3 H); HPLC condition D, 12.27 min, 97.0% 215 nm, 100% 254 nm; condition B, 2.87 min, 93% 215 nm, 95% 254 nm; HRMS calcd for $C_{25}H_{18}Br_2ClN_4O$ 582.9530, found 582.9456.

(±)-*syn*-6,7-Bis(4-bromophenyl)-1-methoxy-2,12-dimethyl-7,12-dihydro-6*H*-chromeno[4,3-*d*][1,2,4]triazolo[1,5-*a*]pyrimidine, 33: Method A (19%), mp 199.5 °C: IR (neat) cm^{-1} 2917, 1645, 1487, 1265, 1090, 1010, 848, 770; ^{1}H NMR (400 MHz, DMSO-d_6) δ ppm 7.73 (s, 1 H), 7.23 (d, J = 8.0 Hz, 3 H), 7.13 (d, J = 7.8 Hz, 2 H), 7.03 (d, J = 8.8 Hz, 1 H), 6.93 (d, J = 8.0 Hz, 2 H), 6.80 (d, J = 8.4 Hz, 2 H), 6.64 (d, J = 8.2 Hz, 1 H), 6.20 (s, 1 H), 5.78 (s, 1 H), 3.87 (s, 4 H), 3.24 (s, 4 H); HRMS (ESI+) m/z 593.0153 (M + H)$^+$; Anal. ($C_{27}H_{23}Br_2N_4O_2$) C, H, N.

(±)-*syn*-6,7-Bis(4-bromophenyl)-3-fluoro-2,12-dimethyl-7,12-dihydro-6*H*-chromeno[4,3-*d*][1,2,4]triazolo[1,5-*a*]pyrimidine, 34: Method A (2%): ^{1}H NMR (400 MHz, DMSO-d_6) δ ppm 7.74 (s, 1 H), 7.59 (d, J = 9.1 Hz, 1 H), 7.11−7.21 (m, 4 H), 6.81 (t, J = 8.1 Hz, 4 H), 6.72 (d, J = 10.2 Hz, 1 H), 5.82 (s, 1 H) 6.08 (s, 1 H), 3.54 (s, 3 H), 2.25 (s, 3 H); HPLC condition C, 5.96 min, 96.1% 210 nm, 95.4% 250 nm; HRMS calcd for $C_{26}H_{20}Br_2FN_4O$ 580.9982, found 580.9906.

(±)-6,7-Bis(4-bromophenyl)-2,4-dichloro-12-methyl-7,12-dihydro-6*H*-chromeno[4,3-*d*][1,2,4]triazolo[1,5-*a*]pyrimidine (1:3 *syn*/*anti*) (35): Method B (44%): ^{1}H NMR (400 MHz, chloroform-*d*) δ ppm 7.73 (s, 1 H, triazole CH, *anti*), 7.69 (s, 1 H, triazole CH, *syn*), 7.61−6.71 (m, 10 H, aromatic H's, *syn* and *anti*), 5.85 (s, 1 H, C6−H, *syn*), 5.78 (s, 1 H, C6−H, *anti*), 5.65 (s, 1 H, C7−H, *syn*), 5.50 (s, 1 H, C7−H, *anti*), 3.64 (s, 3 H, NCH_3, *anti*), 3.62 (s, 3 H, NCH_3, *syn*); HPLC condition A, 6.10, 6.37 min, 1:3 ratio; HRMS calcd for $C_{25}H_{17}Br_2Cl_2N_4O$ 616.9141, found 616.8945.

Chiral Chromatographic Separations and Prediction of Absolute Configuration. The chromenotriazolopyrimidine stereoisomers were purified in multiple injections by preparative Berger Multigram II SFC chromatography using a Chiralcel OJ-H column (250 × 21 mm^2, 5 μm) at 40 °C, 100 psi outlet pressure and isocratic CO_2/methanol 0.1% diethylamine: **1**, 145 mL/min 85:15; **10**, 50 mL/min 80:20; **11**, 65 mL/min 77:23; **19**, 65 mL/min 75:25; **23**, 65 mL/min 70:30; **27**, 60 mL/min 50:50. Computed (B3LYP/6-31G*, *Gaussian 98*) VCD spectra for **1a**−**1d** were compared with those obtained experimentally (BioTools, Inc., Jupiter, FL) allowing for absolute stereochemical assignment.[23]

Acknowledgment. The authors thank Steve Olson and Chris Fotsch for critical revision and Zheng Hua and Wesley Barnhart for chiral separations.

Supporting Information Available: Calculated and experimental VCD data for **1a**, **1b**, **1c**, and **1d**. This material is available free of charge via the Internet at http://pubs.acs.org.

References

(1) (a) Fridman, J. S.; Lowe, S. W. Control of apoptosis by p53. *Oncogene* **2003**, *22*, 9030–9040. (b) Vazquez, A.; Bond, E. E.; Levine, A. J.; Bond, G. L. The genetics of the p53 pathway, apoptosis and cancer therapy. *Nat. Rev. Drug Discovery* **2008**, *7*, 979–987.

(2) (a) Jones, S. N.; Sands, A. T.; Hancock, A. R.; Vogel, H.; Donehower, L. A.; Linke, S. P.; Wahl, G. M.; Bradley, A. The tumorigenic potential and cell growth characteristics of p53-deficient cells are equivalent in the presence or absence of MDM2. *Proc. Natl. Acad. Sci. U.S.A.* **1996**, *93*, 14106–14111. (b) Iwakuma, T.; Lozano, G. Crippling p53 activities via knock-in mutations in mouse models. *Oncogene* **2007**, *26*, 2177–2184. (c) Lozano, G.; Zambetti, G. P. What have animal models taught us about the p53 pathway? *J. Pathol.* **2005**, *205*, 206–220.

(3) (a) Johnston, J. B.; Daeninck, P.; Verburg, L.; Lee, K.; Williams, G.; Israels, L. G.; Mowat, M. R. A.; Begleiter, A. p53, MDM2, BAX and BCL2 and drug resistance in chronic lymphocytic leukemia. *Leuk. Lymphoma* **1997**, *26*, 435–449. (b) Buttitta, F.; Marchetti, A.; Gadducci, A.; Pellegrini, S.; Morganti, M.; Carnicelli, V.; Cosio, S.; Gagetti, O.; Genazzani, A. R.; Bevilacqua, G. p53 alterations are predictive of chemoresistance and aggressiveness in ovarian carcinomas: a molecular and immunohistochemical study. *Br. J. Cancer* **1997**, *75*, 230–235. (c) Harada, T.; Ogura, S.; Yamazaki, K.; Kinoshita, I.; Itoh, T.; Isobe, H.; Yamashiro, K.; Dosaka-Akita, H.; Nishimura, M. Predictive value of expression of p53, Bcl-2 and lung resistance-related protein for response to chemotherapy in non-small cell lung cancers. *Cancer Sci.* **2003**, *94*, 394–399. (d) Yamazaki, Y.; Chiba, I.; Hirai, A.; Ken-ichi, N.; Haruhiko, K.; Kanchu, T.; Yasunori, T.; Tadashi, I.; Takao, K.; Hiroshi, F. Radioresistance in oral squamous cell carcinoma with p53 DNA contact mutation. *Am. J. Clin. Oncol.* **2003**, *26*, e124–e129. (e) Petitjean, A.; Achatz, M. I.; Borresen-Dale, A. L.; Hainaut, P.; Olivier, M. TP53 mutations in human cancers: Functional selection and impact on cancer prognosis and outcomes. *Oncogene* **2007**, *26*, 2157–2165.

(4) Soussi, T.; Dehouche, K.; Beroud, C. p53 web-site and analysis of p53 gene mutations in human cancer: forging a link between epidemiology and carcinogenesis. *Hum. Mutat.* **2000**, *15*, 105–113.

(5) (a) Eymin, B.; Gazzeri, S.; Brambilla, C.; Brambilla, E. MDM2 overexpression and p14ARF inactivation are two mutually

exclusive events in primary human lung tumors. *Oncogene* **2002**, *21*, 2750–2761. (b) Polsky, D.; Bastian, B. C.; Hazan, C.; Melzer, K.; Pack, J.; Houghton, A.; Busam, K.; Cordon-Cardo, C.; Osam, I. HDM2 protein overexpression, but not gene amplification, is related to tumorigenesis of cutaneous melanoma. *Cancer Res*. **2001**, *61*, 7642–7646.

(6) Momand, J.; Mung, D.; Wilczynski, S.; Niland, J. The MDM2 gene amplification database. *Nucleic Acids Res*. **1998**, *26*, 3453–3459.

(7) Michael, D.; Oren, M. The p53-MDM2 module and the ubiquitin system. *Semin. Cancer Biol*. **2003**, *13*, 49–58.

(8) Oliner, J. D.; Kinzler, K. W.; Meltzer, P. S.; George, D.; Vogelstein, B. Amplification of a gene encoding a p53-associated protein in human sarcomas. *Nature* **1992**, *358*, 80–83.

(9) (a) Haupt, Y.; Maya, R.; Kaza, A.; Oren, M. MDM2 promotes the rapid degradation of p53. *Nature* **1997**, *387*, 296–299. (b) Kubbutat, M. H. G.; Jones, S. N.; Vousden, K. H. Regulation of p53 stability by MDM2. *Nature* **1997**, *387*, 299–303. (c) Midgley, C. A.; Lane, D. P. p53 protein stability in tumor cells is not determined by mutation but is dependent on MDM2 binding. *Oncogene* **1997**, *15*, 1179–1189.

(10) (a) Wu, X.; Bayle, J. H.; Olson, D.; Levine, A. J. The p53-MDM2 autoregulatory feedback loop. *Genes Dev*. **1993**, *7*, 1126–1131. (b) Oliner, J. D.; Pietenpol, J. A.; Thiagalingam, S.; Gyuris, J.; Kinzler, K. W.; Vogelstein, B. Oncoprotein MDM2 conceals the activation domain of tumor suppressor p53. *Nature* **1993**, *362*, 857–860. (c) Picksley, S.; Lane, D. The p53-MDM2 autoregulatory feedback loop: A paradigm for the regulation of growth control by p53? *BioEssays* **1993**, *15*, 689–690. (d) Ashcroft, M.; Vousden, K. Regulation of p53 stability. *Oncogene* **1999**, *18*, 7637–7643.

(11) (a) Lane, D. Exploiting the p53 pathway for cancer diagnosis and therapy. *Br. J. Cancer* **1999**, *80* (Suppl 1), 1–5. (b) Chene, P. Inhibiting the p53-MDM2 interaction: an important target for cancer therapy. *Nature Rev. Cancer* **2003**, *3*, 102–109. (c) Bottger, A.; Bottger, V.; Sparks, A.; Liu, W. -L.; Howard, S. F.; Lane, D. P. Design of a synthetic MDM2-binding mini protein that activates the p53 response in vivo. *Curr. Biol*. **1997**, *7*, 860–869.

(12) Carvajal, D.; Tovar, C.; Yang, H.; Vu, B. T.; Heimbrook, D. C.; Vassilev, L. T. Activation of p53 by MDM2 antagonists can protect proliferating cells from mitotic inhibitors. *Cancer Res*. **2005**, *65*, 1918–1924.

(13) (a) Jones, S.; Thornton, J. M. Principles of protein-protein interactions. *Proc. Natl. Acad. Sci. U.S.A*. **1996**, *93*, 13–20. (b) Fry, D. C. Protein-protein interactions as targets for small molecule drug discovery. *Biopolymers* **2006**, *84*, 535–552. (c) Fry, D. C.; Vassilev, L. T. Targeting protein-protein interactions for cancer therapy. *J. Mol. Med*. **2005**, *83*, 955–963.

(14) (a) Clackson, T.; Wells, J. A. A hot spot of binding energy in a hormone-receptor interface. *Science* **1995**, *267*, 383–386. (b) Moreira, I. S.; Fernandes, P. A.; Ramos, M. J. Hot spots - a review of the protein-protein interface determinant amino-acid residues. *Proteins* **2007**, *68*, 803–812.

(15) (a) Vassilev, L. T.; Vu, B. T.; Graves, B.; Carvajal, D.; Podlaski, F.; Filipovic, Z.; Kong, N.; Kammlott, U.; Lukacs, C.; Klein, C.; Fotouhi, N.; Liu, E. A. In vivo activation of the p53 pathway by small-molecule antagonists of MDM2. *Science* **2004**, *303*, 844–848. (b) Parks, D. J.; LaFrance, L. V.; Calvo, R. R.; Milkiewicz, K. L.; Gupta, V.; Lattanze, J.; Ramachandren, K.; Carver, T. E.; Petrella, E. C.; Cummings, M. D.; Maguire, D.; Grasberger, B. L.; Lu, T. 1,4-Benzodiazepine-2,5-diones as small molecule antagonists of the HDM2-p53 interaction: discovery and SAR. *Bioorg. Med. Chem. Lett*. **2005**, *15*, 765–770. (c) Parks, D. J.; LaFrance, L. V.; Calvo, R. R.; Milkiewicz, K. L.; Maruga'n, J. J.; Raboisson, P.; Schubert, C.; Knoblish, H. K.; Zhao, S; Franks, C. F.; Lattanze, J.; Carver, T. E.; Cummings, M. D.; Maguire, D.; Grasberger, B. L.; Maroney, A. C.; Lu, T. Enhanced pharmacokinetic properties of 1,4-benzodiazepine-2,5-dione antagonists of the HDM2-p53 protein-protein interaction through structure-based drug design. *Bioorg. Med. Chem. Lett*. **2006**, *16*, 3310–3314. (d) Ding, K.; Lu, Y.; Nikolovska-Coleska, Z.; Wang, G.; Qiu, S.; Shangary, S.; Gao, W.; Qin, D.; Stuckey, J.; Krajewski, K.; Roller, P. P.; Wang, S. Structure-based design of spiro-oxindoles as potent, specific small-molecule inhibitors of the MDM2-p53 interaction. *J. Med. Chem*. **2006**, *49*, 3432–3435. (e) Hardcastle, I. R.; Ahmed, S. U.; Atkins, H.; Calvert, A. H.; Curtin, N. J.; Farnie, G.; Golding, B. T.; Griffin, R. J.; Guyenne, S.; Hutton, C.; Kallblad, P.; Kemp, S. J.; Kitching, M. S.; Newell, D. R.; Norbedo, S.; Northen, J. S.; Reid, R. J.; Saravanan, K.; Willems, H. M. G.; Lunec, J. Isoindolinone-based inhibitors of the MDM2-p53 protein-protein interaction. *Bioorg. Med. Chem. Lett*. **2005**, *15*, 1515–1520.

(16) (a) Kussie, P. H.; Gorina, S.; Marcchal, V.; Elenbaas, B.; Moreau, J.; Levine, A. J.; Pavletich, N. P. Structure of the MDM2 oncoprotein bound to the p53 tumor suppressor transactivation domain. *Science* **1996**, *274*, 948–953. (b) Garcia-Echeverria, C.; Chene, P.; Blommers, M. J. J.; Furet, P. Discovery of potent antagonists of the interaction between human double minute 2 and tumor suppressor p53. *J. Med. Chem*. **2000**, *43*, 3205–3208.

(17) (a) Hu, C.-Q.; Hu, Y.-Z. Small molecule inhibitors of the p53-MDM2. *Curr. Med. Chem*. **2008**, *15*, 1720–1730. (b) Patel, S.; Player, M. R. Small-molecule inhibitors of the p53-HDM2 interaction for the treatment of cancer. *Expert Opin. Invest. Drugs* **2008**, *17*, 1865–1882.

(18) HTRF data was reported as the mean ± SD at 95% confidence, $n \geq 4$.

(19) LE (ligand efficiency) was calculated based on IC_{50} according to $LE = -RT \ln(IC_{50})/NHA$: Hopkins, A. L.; Groom, C. R.; Alex, A. Ligand efficiency: A useful metric for lead selection. *Drug Discovery Today* **2004**, *9*, 430–431.

(20) A survey of 13 small molecule inhibitors of 7 protein−protein interaction targets had an average LE = 0.24 kcal/mol per non-hydrogen atom: Wells, J. A.; McClendon, C. L. Reaching for high-hanging fruit in drug discovery at protein-protein interfaces. *Nature* **2007**, *450*, 1001–1009.

(21) (a) Desenko, S. M.; Orlov, V. D.; Getmanskii, N. V.; Komykhov, S. A. Imine-enamine tautomerization of dihydroazolopyrimidines 4. Synthesis and tautomerization of 5-(2-hydroxyphenyl)-dihydro-1,2,4-triazolo[1,5-*a*]pyrimidines. *Chem. Heterocycl. Compd*. **1993**, *29*, 1160–1162. (b) Desenko, S. M.; Orlov, N. V.; Getmanskii, N. V.; Komykhov, S. A.; Paponov, B. V.; Kovalevskii, A. Yu.; Shishkin, O. V.; Struchkov, Yu. T. Synthesis and structure of 3,7-dihydro-2H-1,2,4-triazolo-[1′,5′-a′]tripyrimido[4,5-d]benzo[b]pyrans. *Chem. Heterocycl. Compd*. **1996**, *32*, 215–220.

(22) (a) Bunz, F.; Dutriaux, A.; Lengauer, C.; Waldman, T.; Zhou, S.; Brown, J. P.; Sedivy, J. M.; Kinzler, W. K.; Vogelstein, B. Requirement for p53 and p21 to sustain G_2 arrest after DNA damage. *Science* **1998**, *282*, 1497–1501. (b) Waldman, T.; Kinzler, K. W.; Vogelstein, B. p21 is necessary for the p53-mediated G_1 arrest in human cancer cells. *Cancer Res*. **1995**, *55*, 5187–5190.

(23) (a) Stephens, P. J.; Lowe, M. A. Vibrational circular dichroism. *Annu. Rev. Phys. Chem*. **1985**, *36*, 213–241. (b) Polavarapu, P. L.; Zhao, C. Vibrational circular dichroism: a new spectroscopic tool for biomolecular structural determination. *Fresenius' J. Anal. Chem*. **2000**, *366*, 727–734. (c) Stephens, P. J.; Devlin, F. J. Determination of the structure of chiral molecules using ab initio vibrational circular dichroism spectroscopy. *Chirality* **2000**, *12*, 172–179. (d) Freedman, T. B.; Cao, X.; Dukor, R. K.; Nafie, L. A. Absolute configuration determination of chiral molecules in the solution state using vibrational circular dichroism. *Chirality* **2003**, *15*, 743–758. (e) Devlin, F. J.; Stephens, P. J.; Cheeseman, J. R.; Frisch, M. Ab initio prediction of vibrational absorption and circular dichroism spectra of chiral natural products using density functional theory: Camphor and fenchone. *J. Phys. Chem. A* **1997**, *101*, 6322–6333.